Improvement in PbS-based Hybrid Bulk-Heterojunction Solar Cells through Band Alignment via Bismuth Doping in the Nanocrystals

Sudip K. Saha, Abhijit Bera, and Amlan J. Pal*

Department of Solid State Physics, Indian Association for the Cultivation of Science, Jadavpur, Kolkata 700032, India

Ⓢ *Supporting Information*

ABSTRACT: We introduce dopants in lead sulfide (PbS) quantum dots (QDs) in forming hybrid bulk-heterojunction (BHJ) solar cells. Because an increase in the content of bismuth as dopants in PbS QDs transforms the intrinsic *p*-type semiconductor into an *n*-type one, the band alignment between a conjugated polymer and the doped QDs changes upon doping affecting performance of BHJ solar cells. From scanning tunneling spectroscopy (STS) of the doped QDs, we observe a shift in their Fermi energy leading to formation of a type II band alignment in the polymer:doped-QD interface. We also show that the dopants improve electron-conduction process through the QDs. With the dopants controlling both band alignments at the interface and the conduction process, we show that the dopant concentration in QDs influences open-circuit voltage unfavorably and short-circuit current in a beneficial manner. The device performance of hybrid BHJ solar cells is hence maximized at an optimum concentration of bismuth in PbS QDs.

PbS QD

Bi@PbS QD

ITO/PEDOT:PSS/P3HT:QDs/ZnO/Al

KEYWORDS: *Bi-doped PbS quantum dots, shift in Fermi energy, band alignment at polymer:QD interface, effect of doping on hybrid bulk-heterojunction solar cells, electron-conduction through QDs*
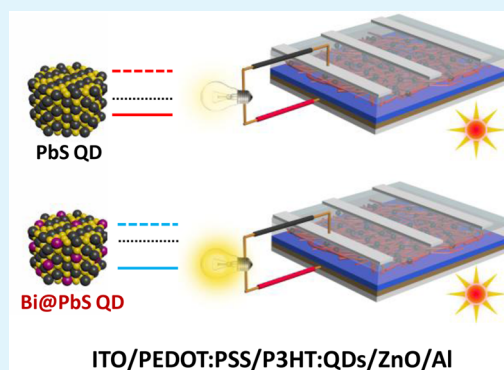
■ INTRODUCTION

Considering certain limitations of conjugated organics in their use in organic photovoltaic devices (OPVs) such as low carrier mobility and extinction coefficient, inorganic semiconductors in the form of quantum dots (QDs) are being incorporated to fabricate hybrid bulk-heterojunction (BHJ) solar cells.[1,2] As in OPVs, the materials in hybrid BHJs are chosen in such a manner that the conduction and valence band-edges (CB and VB, respectively) of QDs and energy levels of conjugated organics form a type II alignment or a staggered gap, so that excitons generated in both the semiconductors are dissociated leading to separation of charge carriers followed by their transport to the opposite electrodes resulting in photocurrent in the external circuit.

Pb-based nanocrystals were considered in this direction primarily due to their extended absorption window to the near-infrared region[2,3] along with the ability to generate multiple excitons.[4] A depleted heterojunction was formed accordingly between PbS, which acted as a *p*-type semiconductor due to oxidation of their surface, and *n*-type nanoparticles (such as TiO_2[5] or ZnO[6]) for *pn*-junction solar cells. The PbS/ZnO structure yielded an energy conversion efficiency exceeding 8%.

Hybrid BHJs with PbS in a conventional polymer matrix, on the other hand, resulted efficiencies under 0.6% due to the *p*-type nature of such polymers and the lack of formation of a type II band alignment.[7−10] Band engineering of PbS has hence become necessary to realize PbS based hybrid BHJ solar cells. The diameter of PbS, even in a quantum confinement regime, is

unlikely to enforce a type II band alignment in the hybrid BHJs. Introduction of heterovalent atoms as dopants in cationic sites of QDs can be an effective route, because a suitable dopant would shift Fermi energy sans an alteration in the bandgap, leading to a change in the nature of the semiconductor and formation of a type II band alignment. True successes came in this endeavor through substitution of heteroatoms at the cationic sites of InAs and of II−VI and IV−VI semiconductor QDs, affecting optical properties and density of states.[11−14] Because PbS nanocrystals would turn into an *n*-type semiconductor upon bismuth doping, Stavrinadis et al. formed *pn*-junctions between the pristine *p*-type PbS and bismuth-doped *n*-type PbS nanocrystals for homojunction solar cell applications.[14] The energy conversion efficiency in such *pn*-junctions ranged up to 2.7%.

Taking a cue from such *pn*-junctions, we aimed to use the doped PbS QDs in forming hybrid BHJs. The level of doping, apart from controlling the conduction processes through the QDs, would influence the band alignment at the polymer:QD interface affecting open-circuit voltage (V_{OC}), short-circuit current (I_{SC}), and other device parameters. In this work, we used bismuth-doped PbS (Bi@PbS) QDs in forming hybrid BHJ solar cells. The conventional polymer, namely, poly(3-hexylthiophene) (P3HT), which is a well-known hole-
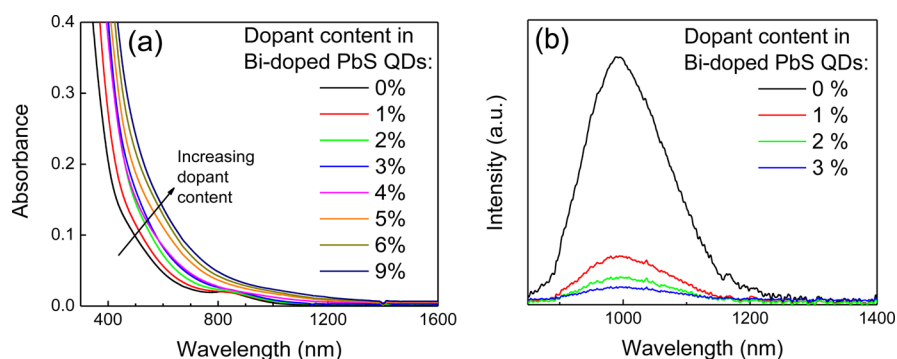
Figure 1. (a) Optical absorption and (b) PL emission spectra of PbS and Bi@PbS QDs in chloroform dispersed solution (1.6 mg/mL). Dopant content in the QDs is specified as legends.

conductor, remained the matrix of the BHJs. We characterized P3HT:Bi@PbS hybrid BHJ devices to study the effect of dopants in the QDs on the parameters of solar cells.

EXPERIMENTAL SECTION

Materials. While oleic acid was purchased from Fluka, 1-octadecene, hexamethyldisilathiane $(CH_3)_3SiSSi(CH_3)_3$, and poly-(3,4-ethylenedioxythiophene)-poly(styrenesulfonate) (PEDOT:PSS, 1.3 wt % dispersion in H_2O) were purchased form Sigma-Aldrich Chemical Co.. Zinc acetate dihydrate $Zn(CH_3COO)_2 \cdot 2H_2O$ and bismuth(III) acetate $(CH_3CO_2)_3Bi$ were purchased from Merck Chemicals and Alfa Aesar, respectively. Electronic-grade poly(3-hexylthiophene-2,5-diyl) (P3HT), which was head-to-tail regioregular (91−94%) and had an average molecular weight (M_w) of 50 000−70 000, was purchased from Rieke Metals, LLC, Lincoln, NE. All the materials were used without further purification.

Growth of PbS Quantum Dots. PbS QDs were grown using a conventional procedure. In brief, PbO was dissolved in 2 mL oleic acid and 10 mL of 1-octadecene to form 1 mmol solution. After degassing the solution for 20 min under a vigorous stirring condition, the temperature of the reaction flask was raised to 150 °C, at which the solution turned transparent and golden yellow in color. The temperature was maintained for 2 h so that lead oleate formed. Without exposing the content of the flask to ambient conditions, the temperature was lowered to 80 °C. At this stage, sulfur solution, formed separately by dissolving 0.1 mL of hexamethyldisilathiane in 10 mL of 1-octadecene, was swiftly injected into the lead oleate solution for the growth of PbS nanocrystals. Within 2 min, the content of the flask turned black, indicating formation of the nanocrystals; the reaction was stopped by a rapid cooling of the flask to room temperature. The PbS nanostructures were separated and purified by adding chloroform/acetone (1:5 v/v) followed by centrifuging thrice at 8000 rpm. The nanocrystals were finally redispersed in chloroform for further use.

Bismuth Doping in PbS QDs. Bismuth-doped PbS (Bi@PbS) nanocrystals were grown following a reported procedure.[14] In brief, a measured amount of bismuth acetate was added to PbO, so that bismuth oleate formed along with lead oleate. The addition of sulfur precursor, as followed during the growth of pristine PbS QDs, resulted in the formation of bismuth-doped PbS nanocrystals. In this work, we varied the bismuth content in PbS QDs by varying the amount of bismuth acetate in the reaction.

Growth of ZnO Nanocrystals. ZnO nanocrystals were grown through hydrolysis and condensation of zinc acetate dihydrate, $Zn(CH_3COO)_2 \cdot 2H_2O$, at 65 °C by slow addition of potassium hydroxide in methanol following a standard process. The nanocrystals were separated after cooling the flask down to room temperature, followed by washing in methanol/n-butanol (1:5 v/v) two times.

Characterization of Nanoparticles. PbS and different Bi@PbS QDs and ZnO nanocrystals were characterized by recording their optical absorption and photoluminescence (PL) spectroscopy in the UV−visible−NIR region, X-ray diffraction (XRD) patterns, trans-

mission electron microscopy (TEM) and high-resolution TEM (HR-TEM) images, and X-ray photoelectron spectroscopy (XPS). The measurements were carried out with a Varian 5000 UV−vis−NIR Spectrophotometer, Jobin Yvon iHR320 Imaging Spectrometer, Bruker D8 Advanced X-ray Powder Diffractometer, JEM 2100F Jeol TEM, and an XPS instrument (Omicron: serial no. 0571), respectively. In addition, to substantiate the n-type nature Bi@PbS QDs and also the p-type nature of PbS QDs, we have recorded their scanning tunneling spectrocopy (STS). Tunneling current was measured through an ultrathin layer of the QDs formed on doped silicon substrates with a PAN-style ultrahigh vacuum scanning tunneling microscope (UHV-STM) manufactured by M/s RHK Technologies, Troy, MI. The base pressure of the microscope chamber was kept at 2.7×10^{-10} mbar. A platinum/iridium (Pt/Ir, 80/20%) wire was mechanically cut to form STM tips to record tunneling current of the QDs. Bias was applied to the substrate-electrode. During an approach of the tip, a preset current was achieved at 2.0 V through a feedback loop of the STM controller.

Device Fabrication. Devices were fabricated on glass substrates coated with indium tin oxide (ITO). The ITO electrodes, which were striped and had a surface resistance of 14 Ω/square, were washed using a standard protocol. They were treated with UV ozone cleaner (Novascan Technologies, Inc.) for 20 min before fabrication of the devices. First, PEDOT:PSS was spun on the ITO substrates at 2000 rpm for 60 s followed by annealing of the film in a tube furnace at 120 °C for 30 min in an ambient condition. PEDOT:PSS coated substrates were transferred to a glovebox for the deposition of subsequent layers. Undoped PbS and different Bi@PbS QDs were first mixed with P3HT in chloroform, because both components were well-soluble in the solvent. The amount of QDs in P3HT was 1:1 w/w in all the cases. To spun the active layer, P3HT:QD solution (10 mg/mL) was spun at 2000 rpm for 60 s followed by annealing at 140 °C for 30 min. Thickness of the active layer, as evaluated by recording atomic force microscopy (AFM) of a depth profile of an intentional scratch on a separate film, was 70 nm. On top of the active layer, a thin-film of ZnO nanocrystals was spun from methanol solution at 2000 rpm for 60 s followed by annealing at 140 °C for another half hour. To complete fabrication of devices, aluminum (Al) as a top electrode was thermally evaporated at 2×10^{-6} mbar at a speed of 0.4 Å/s. Overlap of ITO and Al strips defined the area of the devices (6.35 mm²).

Device Characterization. The solar cells were characterized in the glovebox that was fitted with a solar simulator. Simulated solar illumination was obtained from a Newport-Stratfort 300 W Solar Simulator. Intensity of solar illumination was varied by using neutral density filters. A Keithley 2636A Electrometer were used to measure current−voltage ($I-V$) characteristics of the devices in a dark condition and under a range of illumination intensities. We have used a mask to ensure that the areas outside the cell did not receive light during the measurement. While the step-voltage was 0.04 V, sweep-speed was kept low (10 mV/s) to minimize the effect of displacement current. Real and imaginary component of complex impedance were recorded with a Solartron 1260A Impedance Analyzer. Eight data points were recorded per decade of frequency.
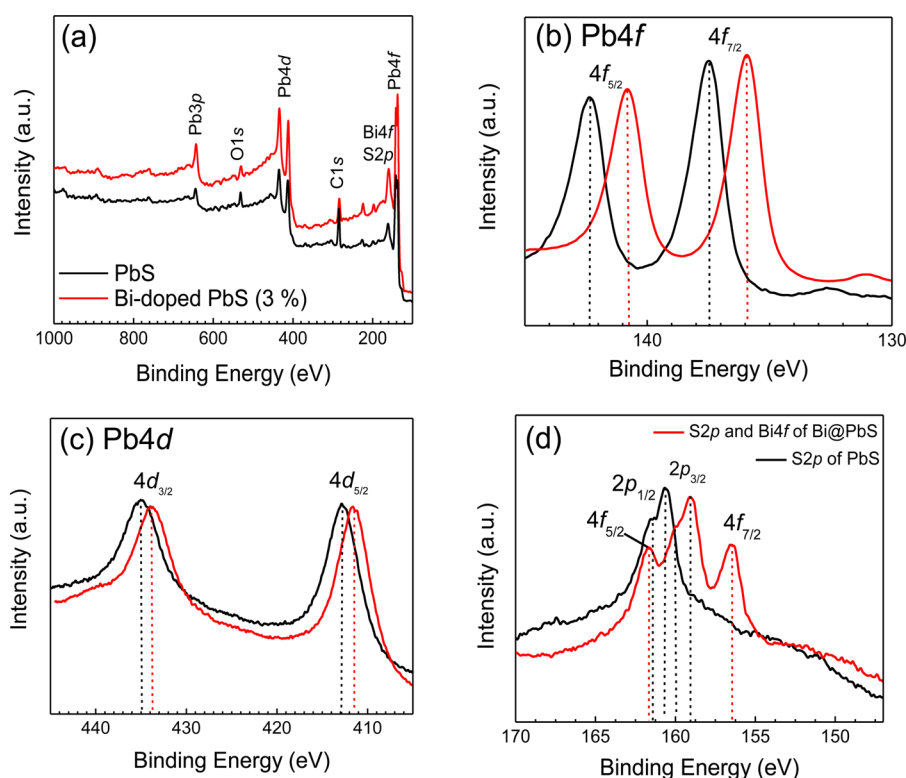
Figure 2. (a) Full-range XPS spectrum of undoped and Bi@PbS (3%) QDs. High-resolution spectra of the QDs to resolve (b) Pb 4f, (c) Pb 4d, and (d) S 2p levels. In panel d, Bi 4f levels appearing due to the dopants in the doped QDs are also shown.

A 100 mV rms was used as a test ac voltage to record the complex impedance; no dc voltage was applied to the devices during the measurements. To record external quantum efficiency (EQE) spectrum of the solar cells, a Jobin-Yvon H20 IR and a Cornerstone 130 monochromator were used to disperse the solar illumination.

■ RESULTS AND DISCUSSION

Characteristics of PbS and Bi-doped PbS QDs. The pristine and doped PbS QDs were characterized following usual methods. Optical absorption spectra of different QDs having Bi/Pb ratio ranging from 0 to 9% are presented in Figure 1a. For the undoped PbS and Bi@PbS with low dopant content, the spectra show a continuum in the high-energy region along with an excitonic transition at around 820 nm. With an increase in the doping content, the excitonic peak that appeared due to defect states merges with the continuum since bismuth occupied the vacant sites in the QDs. PL spectra of the QDs in dispersed solution with an excitation wavelength of 650 nm are shown in Figure 1b. The PL emission of PbS QDs at 996 nm appeared primarily due to states arising out of vacant sites in pristine PbS. Upon bismuth doping, the emission progressively quenched due to filling of the optically accessible states of QDs. Both the optical absorption and PL emission spectra of pristine and Bi@PbS QDs matched the reported results.

To obtain further insights on bismuth doping in PbS QDs, we recorded their XRD patterns at different level of doping. Figure S1 (Supporting Information) clubs such spectra for different content of bismuth in the QDs. The diffraction peaks of PbS QDs are in concurrence with that of rock salt PbS crystals (JCPDS file 05-0592). The peaks for the Bi@PbS QDs quietly matched with the ones of undoped PbS. A careful analysis of the XRD spectra shows a small but systematic shift

of the peaks corresponding to ⟨111⟩ plane of PbS crystals toward the smaller angle. The shift, amounting to less than half a degree when the content of diffused bismuth in PbS was the highest, would occur if lead ions were replaced by a slightly larger bismuth ions. To rule out formation of Bi_2S_3 in the QDs, we compared XRD spectra of Bi@PbS QDs and Bi_2S_3 nanocrystals grown separately. The peaks in the XRD spectrum of Bi_2S_3 nanocrystals and the reported results of the material were not present in the spectra of bismuth-doped PbS QDs. Hence, we can infer that bismuth inoculation during the synthesis process did not produce other phases with excess lead remaining unreacted. This is in accordance with previous findings on this system.[14]

To characterize the undoped and Bi@PbS QDs, we have recorded their TEM images (Figure S2, Supporting Information). The TEM images evidenced spherical nature of most of the QDs. HR-TEM images of the QDs, as presented along with TEM images, bring out the lattice fringes with a d-spacing of 0.3 nm. The value matches the spacing of ⟨200⟩ planes (JCPDF file 05-0592) of PbS crystals and did not vary upon bismuth doping in the QDs. To know the degree of monodispersivity of the QDs, we have presented a histogram of diameter distribution calculated from measurements of diameters of 150 or more particles (Figure S2, Supporting Information). Average diameter of PbS and Bi-doped PbS (3%) QDs turned out to be 3.2 and 3.1 nm, respectively. We can therefore infer that there was practically no change in the diameter upon bismuth doping. This is in agreement with the previously reported result.[14]

To gather information about the valence state of elements and elemental composition of the PbS and Bi@PbS QDs, we carried out their XPS measurements (Figure 2). Binding energies obtained in XPS analyses were corrected with respect
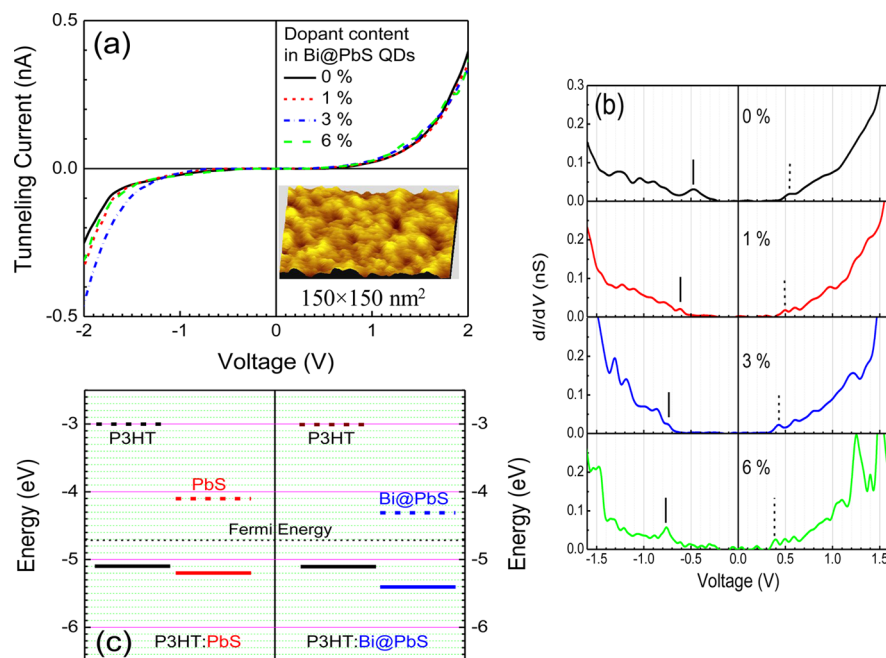
Figure 3. (a) Current−voltage and (b) differential conductance (dI/dV) plots of PbS and bismuth-doped PbS QDs. Dopant content in the QDs is specified as legends. Conduction band (CB) and valence band (VB) edges of the QDs are marked in the DOS spectra as vertical lines in the positive and the negative voltages, respectively. (a, inset) Typical STM topography of an ultrathin film of PbS QDs. (c) Energy diagram of BHJs based on P3HT:QDs before and after bismuth doping in the QDs sandwiched between ITO and Al electrodes.

to C1s peak at 284.5 eV. Full spectra of PbS and Bi@PbS QDs are presented in Figure 2a. The doping concentration chosen in the plot was 3%. Presence of Pb 4f, Pb 4d, Pb 3p, and S 2p states at specified energies confirmed the occurrence of Pb^{2+} and S^{2-} states in PbS and in doped QDs. In Figure 2b, we further show that the Pb 4f of both the QDs resolved into $4f_{7/2}$ and $4f_{5/2}$. Similarly, as shown in Figure 2c, Pb 4d level resolved into $4d_{5/2}$ and $4d_{3/2}$. The 4f and 4d levels of Pb in Bi@PbS QDs underwent a shift of around 1.5 and 1.1 eV, respectively, toward the low energy region when compared with the respective spectrum of pristine PbS QDs. Such shifts are in concurrence with the XRD results, which also exhibited a shift toward the smaller angle upon doping with slightly larger bismuth ions. The shift in XPS peak positions upon doping are in agreement with the XPS results observed in nitrogen-doped TiO$_2$ nanoparticles and in brominated graphene.[15,16]

The levels of sulfur (S 2p), as presented in Figure 2(d), resolved into $2p_{1/2}$ and $2p_{3/2}$ confirming formation of Pb^{2+}S^{2-} in the QDs. In bismuth-doped PbS QDs, the binding energies of Bi 4f states lie in the S 2p region. Hence, the spectrum of doped PbS QDs in the 150−170 eV regions show Bi 4f levels in addition to S 2p levels of the QDs. The figure furthermore shows that while the S 2p level of both the QDs resolved into $2p_{1/2}$ and $2p_{3/2}$, the 4f level of bismuth in doped PbS resolved into $4f_{7/2}$ and $4f_{5/2}$ confirming formation of Pb$^{2+}_{1-\delta}$Bi$^{3+}_{\delta}$S^{2-} and hence a possible n-nature of doping in PbS QDs. Here δ represent the content of dopants in Bi@PbS QDs. The calculated Bi/Pb ratio from the XPS spectra was found to be approximately 3%. The doping content as obtained from XPS analyses matches well with that expected from the weight of bismuth oleate added to the reaction flask during the growth of the doped QDs.

Scanning Tunneling Spectroscopy (STS) of PbS and Bi@PbS QDs: Density of States. To add credence to the fact that the QDs became n-type in nature upon bismuth doping,

we recorded STS of the QDs. We chose a range of dopant concentrations to record the STS. A typical STM topography of Bi@PbS QDs is presented in the inset of Figure 3a. Tunneling current versus voltage ($I−V$) characteristics of undoped and doped QDs are shown in the figure. The characteristics pass through the set-point (+1.5 V, 0.1 nA) at which the approach of the STM was achieved before recording the tunneling current. The current at regions away from the set-points depended on the dopant concentration of the QDs.

From STS, we have calculated differential conductance (dI/dV) that has correspondence to the density of states (DOS) of the QDs. With bias being applied to the substrate with respect to the tip, a positive voltage meant injection of electrons to the QDs. At negative voltages, electrons could be withdrawn from the QDs. From the dI/dV spectra, conduction and valence band-edges could therefore be located in the form peaks in the positive and the negative voltages, respectively. The CB and VB edges along with the location of Fermi energy, which is considered to be aligned at 0 V, thereby would infer the nature of the QDs.

DOS of QDs as a function of dopant-concentration is shown in Figure 3b. The figure shows that in undoped QDs, Fermi energy was located closer to the VB edge inferring their p-type nature. The spectra moreover show that upon bismuth doping, the Fermi energy shifted toward the conduction band-edge. The results hence support the transformation of PbS QDs to an n-type semiconductor upon bismuth doping. In the QDs with a higher doping level (6%), some weak peaks appeared in the negative voltage within the bandgap. They may represent signature of possible trap states close to the valence band-edge of the QDs.

A shift in the Fermi energy upon doping of PbS QDs with bismuth is expected to favor formation of a type II band alignment when a hybrid bulk heterojunction between the doped-QDs and P3HT was formed. The surmise is due to the
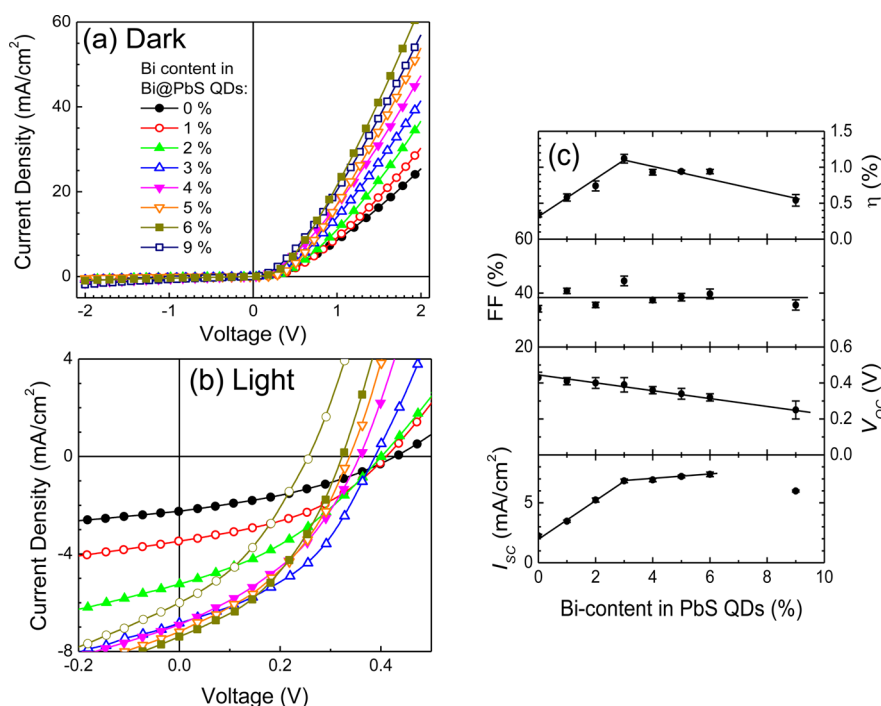
Figure 4. Current−voltage characteristics of P3HT:QD BHJ devices under (a) a dark and (b) a 1 Sun white light illumination condition. Content of bismuth in Bi-doped PbS (Bi@PbS) QDs was varied from 0 to 9%. (c) Plots of short-circuit current (I_{SC}), open-circuit voltage (V_{OC}), fill factor (FF), and energy conversation efficiency (η) of BHJ solar cells based P3HT:QDs as a function of bismuth-content in Bi@PbS QDs. Average values of the parameters measured in four cells were plotted along with their standard deviations as error bars.

fact that the shift of Fermi energy toward the CB would allow the QDs to accept electrons from the polymer. Since the polymer will also be able to accept holes from the QDs, dissociation of excitons generated in both the materials would remain possible. Energy diagrams of BHJs based on P3HT:QDs before and after bismuth doping in the QDs are shown in Figure 3c elaborating formation of a better type II band alignment in P3HT:Bi@PbS hybrid BHJs. Here, we considered the BHJs to be sandwiched between ITO and aluminum electrodes to formulate the energy diagram of the device in an "after contact" configuration.

Hybrid BHJ Solar Cells based on PbS and Bi@PbS QDs in P3HT Matrix. Formation of a type II band alignment at the P3HT:QD interface upon bismuth doping in PbS QDs can best be demonstrated by recording photovoltaic characteristics of the devices. We therefore characterized the P3HT:QD hybrid BHJ devices. As for the QDs, we chose seven different bismuth contents as the doping level, apart from the undoped PbS nanocrystals. In Figure 4, we plot I−V characteristics of the devices under dark and an illumination condition of 1 Sun.

Under a dark condition, I−V characteristics of the devices were rectifying in nature. Such a nature appeared due to the dissimilar work-function of the metal electrodes used to sandwich the active layer. The current was higher at a positive voltage because a bias was applied to the higher work-function metal (ITO) as compared the lower one (Al). Upon an increase in bismuth-content in the QDs, conductivity of P3HT:QDs primarily increased. In the BHJ devices, while hole conduction is primarily through the polymer, the QDs are expected to be responsible for electron-conduction, which would be improved when the QDs become n-type in nature. That is, in BHJs based on doped-PbS, both types of carriers would contribute to the conduction process, resulting in an increase in the device current. The increased conductance in

doped PbS would also offer an efficient electron extraction from the devices upon photoillumination and, hence, a better photovoltaic response.

I−V characteristics of the BHJ devices under 1 Sun are shown in Figure 4b. All the devices under illumination acted as solar cells. As expected, the V_{OC}, I_{SC}, and other device parameters depended on the dopant content in the QDs. In Figure 4c, we have collated the parameters as a function of bismuth content in the doped QDs. The figures show that an increase in the Bi content led to a decrease in V_{OC} and an increase in I_{SC}. With the change in fill factor (FF) being marginal, the BHJ devices with 3% bismuth in PbS QDs yielded an optimum energy conversion efficiency (η). The decrease in V_{OC} could be explained due to the shift in the Fermi energy upon Bi doping. The doping led to a decrease in the energy difference between the HOMO of electron donor (P3HT) and the conduction band of the QDs in an "after contact" configuration determining the V_{OC} of a BHJ solar cell. The increase in I_{SC} occurred for two reasons: (1) improved exciton dissociation due to formation of a type II band alignment at the interface between P3HT and doped PbS and (2) an increased electron-conduction process through the doped QDs for a better extraction of electrons upon photogeneration. The two dependences, namely, a decrease in V_{OC} and an increase in I_{SC} upon bismuth-doping, have opposing effects on η; while the decrease in V_{OC} is detrimental to solar cells, the increased I_{SC} is naturally advantageous to η. We therefore observed that the η maximized to 1.12% at an optimum content of bismuth in PbS QDs. Recall that the reported η of BHJs based on undoped PbS was less than 0.6%. Hence, the results highlight the importance of doping content in QDs in hybrid BHJ solar cells. It may be recalled that the dopants affected conductivity and energy diagram of hybrid BHJ devices.

We varied the intensity of illumination while recording the photovoltaic properties. Characteristics of hybrid BHJ solar cells based on 3% bismuth-doped PbS QDs in P3HT matrix under white light illumination of different intensities have been summarized in Figure 5. While the I_{SC} expectedly increased
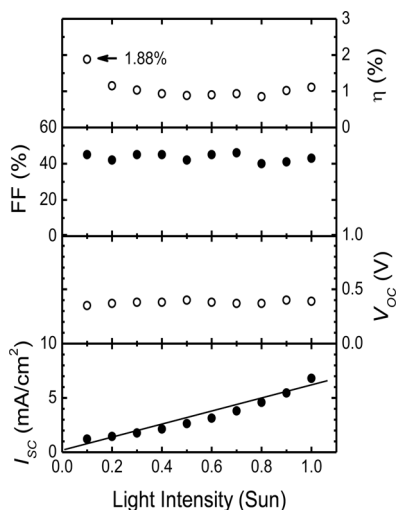

Figure 5. Plots of short-circuit current (I_{SC}), open-circuit voltage (V_{OC}), FF, and energy conversation efficiency (η) of a BHJ solar cells based on 3% bismuth-doped PbS QDs in P3HT matrix as a function of the intensity of while light illumination.

with the intensity, the change in V_{OC} and fill factor was marginal. The energy conversion efficiency on the other hand showed a higher value at a low illumination intensity reaching up to 1.88%. Parameters of BHJ devices based on QDs having other doping contents behaved in a similar manner with the intensity of illumination.

It is imperative to know if excitons generated both in QDs and polymer contributed to photocurrent. We therefore recorded external quantum efficiency (EQE) spectrum by measuring the photocurrent response under a monochromatic light. EQE spectra of some representative BHJ solar cells are shown in Figure 6. For comparison, we have added the optical absorption spectrum of a thin-film comprising of PbS QDs in P3HT. The spectral response of EQE and optical absorption spectrum matched well implying that the photons generated
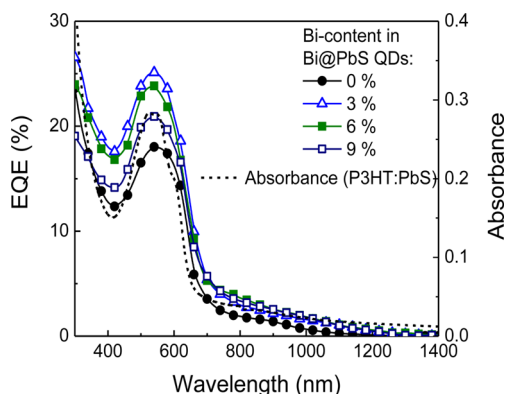

Figure 6. External quantum efficiency (EQE) spectra of BHJ solar cells based on undoped and bismuth-doped PbS QDs in P3HT. Optical absorption spectrum of P3HT:PbS thin-film is shown in the right scale of the plot.

both in QDs and P3HT contributed to photocurrent. The peak intensity corresponded well with η of the devices when widening of the EQE spectrum was considered. The contribution of QDs in the low wavelength region of EQE spectra was higher implying that excitons generated in the QDs must have been dissociated favorably as compared to those generated in the polymer. The EQE spectrum of the device based on 3% bismuth-doped PbS was higher than that of the other devices. The results are hence in concurrence with the I–V characteristics under illumination or photovoltaic properties of the devices.

Impedance Spectroscopy. We have recorded impedance spectroscopy of the hybrid BHJ devices under dark conditions and illumination. Real and imaginary component of complex impedance of the sandwiched structures were recorded as a function of the frequency (f) of test voltage. No dc bias was applied during the measurements. Impedance spectroscopy has begun to be used in P3HT:fullerene BHJ OPVs and in hybrid BHJs based on inorganic semiconductor QDs in a polymer matrix.[17,18] Nyquist plots of the devices, as shown in Figure 7, are semicircular in nature, suggesting that the devices could be modeled to a combination of a resistor and a capacitor in a parallel configuration (C_P–R_P). The diameter of the semicircle with the abscissa represents the resistance (R_P) of the device. R_P decreased with increased bismuth content in QDs, implying increased conductance in P3HT:QDs upon bismuth doping in PbS. The results are in concurrence with the I–V characteristics under a dark condition (Figure 4a). The semicircles intercepted the real component of impedance (Z') axis also near the origin of the coordinate (high frequency region). The intercept, which is a measure of a resistance (R_S) in series with the C_P–R_P combination, represents a contact resistance with the electrodes, which did not vary upon illumination.

Upon illumination, R_P of all the devices decreased sharply. The decrease in R_P is primarily due to the introduction of charge carriers. The frequency at the apex of a Nyquist plot represents characteristic angular frequency (ω) of the device. The frequency increased by more than 1 order of magnitude when the devices were illuminated (Table 1). The frequency, which represents the time constant of internal charge transfer at the polymer:QD interface, increased upon an increase in bismuth content in QDs. Due to doping, the P3HT:Bi@PbS junction forms a better type II band alignment, thereby facilitating charge separation upon photoillumination. An efficient charge separation at the polymer:Bi@PbS interface leading to a higher carrier concentration in illuminated devices is manifested by an increased ω upon an increase in bismuth content in the QDs.

■ CONCLUSION

In conclusion, we have fabricated hybrid BHJ solar cells based on bismuth doped PbS QDs in P3HT matrix. From STS and correspondingly DOS of the QDs, we have observed that upon doping, Fermi energy of the QDs shifted toward the conduction band-edge. This resulted transformation of the p-type PbS QDs to n-type Bi-doped PbS QDs. Such a transformation led to an increased electrical conductivity through the doped QDs and, more importantly, formation of a type II band alignment at the polymer:QD interface favoring photovoltaic performance of the hybrid BHJ solar cells. We have inferred that upon bismuth doping the shift in the Fermi energy of QDs resulted in a decrease in V_{OC}; the doping also yielded a favorable type II band alignment facilitating exciton-
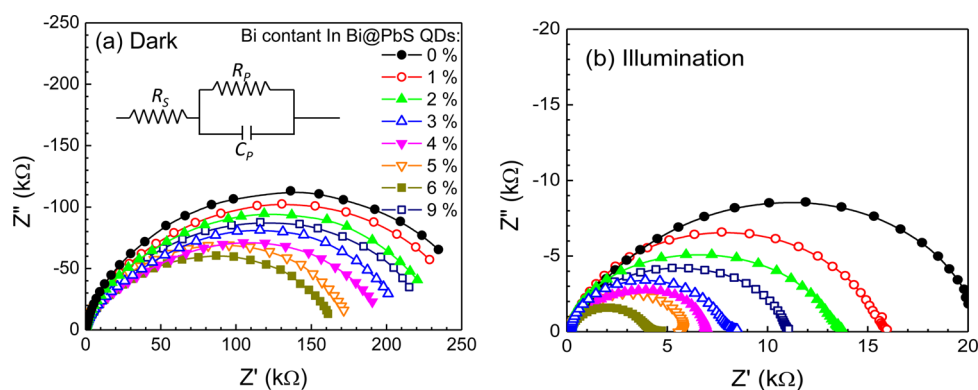
Figure 7. Plots of real and imaginary component of complex impedance (Z′ and Z″, respectively) of P3HT:QD BHJ devices under (a) dark conditions and (b) 1 Sun white light illumination. Content of bismuth in Bi-doped PbS (Bi@PbS) QDs was varied from 0 to 9%. (a, inset) Equivalent electrical analogue prevalent to sandwiched structures.

Table 1. Parameters of the Equivalent Electrical Analogue of P3HT:QD BHJ Devices under Dark Conditions and Illumination

Bi content (%) in Bi@PbS QDs in P3HT:QD BHJ devices	under dark conditions			under illumination		
	R_S (Ω)	R_P (kΩ)	f (Hz)	R_S (Ω)	R_P (kΩ)	f (Hz)
0	125	272	39	142	20	631
1	120	261	50	134	15	1000
2	160	237	63	146	13	1585
3	131	232	79	120	8	2512
4	192	209	100	152	7	3162
5	160	180	125	138	6	3981
6	181	165	158	145	4	6310
9	222	232	63	150	11	1995

dissociation and an increased conductivity for extraction of electrons through the QDs thereby resulting in an increase in I_{SC}. The energy conversion efficiency of the solar cells therefore responded to the doping content in PbS QDs and maximized at an optimum bismuth concentration.

ASSOCIATED CONTENT

Supporting Information

XRD spectra of PbS and Bi-doped PbS QDs, TEM and HR-TEM images and histogram of diameter distribution of PbS, and 3% Bi-doped PbS QDs. This material is available free of charge via the Internet at http://pubs.acs.org.

AUTHOR INFORMATION

Corresponding Author
*Tel: +91-33-24734971. Fax: +91-33-24732805. E-mail: sspajp@iacs.res.in.

Notes
The authors declare no competing financial interest.

ACKNOWLEDGMENTS

REFERENCES

(1) Huynh, W. U.; Dittmer, J. J.; Alivisatos, A. P. Hybrid Nanorod−Polymer Solar Cells. *Science* **2002**, *295*, 2425−2427.

(2) Gunes, S.; Fritz, K. P.; Neugebauer, H.; Sariciftci, N. S.; Kumar, S.; Scholes, G. D. Hybrid Solar Cells using PbS Nanoparticles. *Sol. Energy Mater. Sol. Cells* **2007**, *91*, 420−423.

(3) McDonald, S. A.; Konstantatos, G.; Zhang, S. G.; Cyr, P. W.; Klem, E. J. D.; Levina, L.; Sargent, E. H. Solution-Processed PbS Quantum Dot Infrared Photodetectors and Photovoltaics. *Nat. Mater.* **2005**, *4*, 138−U114.

(4) Ellingson, R. J.; Beard, M. C.; Johnson, J. C.; Yu, P. R.; Micic, O. I.; Nozik, A. J.; Shabaev, A.; Efros, A. L. Highly Efficient Multiple Exciton Generation in Colloidal PbSe and PbS Quantum Dots. *Nano Lett.* **2005**, *5*, 865−871.

(5) Pattantyus-Abraham, A. G.; Kramer, I. J.; Barkhouse, A. R.; Wang, X. H.; Konstantatos, G.; Debnath, R.; Levina, L.; Raabe, I.; Nazeeruddin, M. K.; Gratzel, M.; Sargent, E. H. Depleted-Heterojunction Colloidal Quantum Dot Solar Cells. *ACS Nano* **2010**, *4*, 3374−3380.

(6) Chuang, C. H. M.; Brown, P. R.; Bulovic, V.; Bawendi, M. G. Improved Performance and Stability in Quantum Dot Solar Cells through Band Alignment Engineering. *Nat. Mater.* **2014**, *13*, 796−801.

(7) Seo, J.; Kim, S. J.; Kim, W. J.; Singh, R.; Samoc, M.; Cartwright, A. N.; Prasad, P. N. Enhancement of the Photovoltaic Performance in PbS Nanocrystal:P3HT Hybrid Composite Devices by Post-Treatment-Driven Ligand Exchange. *Nanotechnology* **2009**, *20*, 095202.

(8) Noone, K. M.; Strein, E.; Anderson, N. C.; Wu, P. T.; Jenekhe, S. A.; Ginger, D. S. Broadband Absorbing Bulk Heterojunction Photovoltaics Using Low-Bandgap Solution-Processed Quantum Dots. *Nano Lett.* **2010**, *10*, 2635−2639.

(9) Guchhait, A.; Rath, A. K.; Pal, A. J. Near-IR Activity of Hybrid Solar Cells: Enhancement of Efficiency by Dissociating Excitons Generated in PbS Nanoparticles. *Appl. Phys. Lett.* **2010**, *96*, 073505.

(10) Firdaus, Y.; Vandenplas, E.; Justo, Y.; Gehlhaar, R.; Cheyns, D.; Hens, Z.; Van der Auweraer, M. Enhancement of the Photovoltaic Performance in P3HT:PbS Hybrid Solar Cells Using Small Size PbS Quantum Dots. *J. Appl. Phys.* **2014**, *116*, 094305.

(11) Mocatta, D.; Cohen, G.; Schattner, J.; Millo, O.; Rabani, E.; Banin, U. Heavily Doped Semiconductor Nanocrystal Quantum Dots. *Science* **2011**, *332*, 77−81.

(12) Liu, H.; Zhitomirsky, D.; Hoogland, S.; Tang, J.; Kramer, I. J.; Ning, Z. J.; Sargent, E. H. Systematic Optimization of Quantum Junction Colloidal Quantum Dot Solar Cells. *Appl. Phys. Lett.* **2012**, *101*, 151112.

(13) Sahu, A.; Kang, M. S.; Kompch, A.; Notthoff, C.; Wills, A. W.; Deng, D.; Winterer, M.; Frisbie, C. D.; Norris, D. J. Electronic Impurity Doping in CdSe Nanocrystals. *Nano Lett.* **2012**, *12*, 2587−2594.

(14) Stavrinadis, A.; Rath, A. K.; de Arquer, F. P. G.; Diedenhofen, S. L.; Magen, C.; Martinez, L.; So, D.; Konstantatos, G. Heterovalent Cation Substitutional Doping for Quantum Dot Homojunction Solar Cells. *Nat. Commun.* **2013**, *4*, 2981.

(15) Tongay, S.; Schumann, T.; Miao, X.; Appleton, B. R.; Hebard, A. F. Tuning Schottky Diodes at the Many-Layer-Graphene/Semiconductor Interface by Doping. *Carbon* **2011**, *49*, 2033−2038.

(16) Chen, X. B.; Burda, C. Photoelectron Spectroscopic Investigation of Nitrogen-Doped Titania Nanoparticles. *J. Phys. Chem. B* **2004**, *108*, 15446−15449.

(17) Garcia-Belmonte, G.; Boix, P. P.; Bisquert, J.; Sessolo, M.; Bolink, H. J. Simultaneous Determination of Carrier Lifetime and Electron Density-of-States in P3HT:PCBM Organic Solar Cells under Illumination by Impedance Spectroscopy. *Sol. Energy Mater. Sol. Cells* **2010**, *94*, 366−375.

(18) Leever, B. J.; Bailey, C. A.; Marks, T. J.; Hersam, M. C.; Durstock, M. F. In Situ Characterization of Lifetime and Morphology in Operating Bulk Heterojunction Organic Photovoltaic Devices by Impedance Spectroscopy. *Adv. Energy Mater.* **2012**, *2*, 120−128.